

Design of Compact, Wideband Dual-Polarized Multi-Dipole Antenna for 2G/3G/LTE Base Station Applications

Zhaoyang Tang*, Yapeng Li, Zhipeng Zhao, and Yingzeng Yin

Abstract—In this paper, a wideband dual-polarized multi-dipole antenna with a compact radiator size is developed for 2G/3G/LTE base station applications. The original antenna is composed of a pair of crossed square loop dipoles (SLDs) and two big Y-shaped feeding lines. Thanks to the adopted capacitive coupling, a wide impedance bandwidth is obtained with dual resonant modes in the low and middle frequency bands. Owing to the circular chamfers in the crossed SLDs, the dual resonant modes are away from each other. Thus, a compact radiator size is implemented, and it is about $0.382\lambda_0 \times 0.382\lambda_0$ (λ_0 is the wavelength at center frequency of operation). To further widen the operating bandwidth of the antenna, a pair of crossed rectangular loop dipoles (RLDs) and four small Y-shaped feeding lines are introduced to generate a new resonant mode at high frequency. As a result, the impedance bandwidth of the proposed antenna is enhanced. Based on the optimized dimensions of the simulated antenna model, a prototype is developed, fabricated and tested. Measured results show that the proposed antenna has a relative impedance bandwidth of 53.9% from 1.68 to 2.92 GHz at two ports for $VSWR < 1.5$. Within the operating impedance bandwidth, the measured port-to-port isolation is better than 30 dB. In addition, a stable gain of 8.2 ± 0.5 dBi and a stable radiation pattern with $66^\circ \pm 4^\circ$ half-power beamwidth (HPBW) in the horizontal plane are achieved across the whole bandwidth of operation for dual polarizations. Finally, the proposed antenna is suitable for base station applications.

1. INTRODUCTION

Acting as a device of receiving and transmitting electromagnetic signals, an antenna becomes more and more important in the modern communication systems. In order to suppress the multi-path fading effect and increase the channel capacity [1], antennas with polarization diversity have been widely applied in base station applications. Moreover, designing a wideband antenna has been an increased interest because it can save installation space and reduce cost of the equipment. Thus, the characteristics of wide impedance bandwidth and polarization diversity are essential for base station antennas.

In recent years, a large number of wideband antennas with polarization diversity have been developed. Crossed printed dipole antennas with different feeding techniques such as coaxial probe [2], Y-shaped feeding lines [3, 4], and printed baluns [5–7] are used in base station applications because of wide operating bandwidth, light weight and low cost. Patch antennas are another classic wideband antenna type [8, 9]. However, their operating bandwidths cannot meet requirements of 1.71–2.69 GHz for $VSWR < 1.5$. Magneto-electric dipole antennas are new kinds of wideband antennas by combining electric and magnetic dipoles [10–12]. Nevertheless, the weight of these antennas is too heavy due to the metal structure. A dual-polarized antenna with loaded multi-dipoles was proposed in 2015 [13]. Measured results show that a wide impedance bandwidth, high port isolation, and good radiation performance are obtained for the antenna. However, there is difficulty to massively assemble due to its

Received 19 December 2018, Accepted 23 January 2019, Scheduled 30 January 2019

* Corresponding author: Zhaoyang Tang (zhaoyangt@126.com).

The authors are with the National Key Laboratory of Antennas and Microwave Technology, Xidian University, Xi'an, Shaanxi 710071, China.

3-D structure. By exciting the crossed slot loaded inductors, the dual-polarized antenna in [14] achieves a wide impedance bandwidth and high port isolation. However, the main drawback for the reported antenna is that the radiator size is too large.

In this paper, a wideband dual-polarized multi-dipole antenna with a compact radiator size is proposed for base station applications. To reduce the radiator size, circular chamfers are introduced in crossed SLDs. In addition, operating impedance bandwidth of the proposed antenna is significantly enhanced by loading a pair of crossed RLDs and four small Y-shaped feeding lines. A prototype of the proposed antenna is designed, fabricated, and tested. Measured results demonstrate that some superior performances are achieved for the proposed antenna, such as wide impedance bandwidth, high port isolation, stable gain, and stable radiation pattern. Detailed discussions about the antenna design are presented as follows.

2. DUAL-POLARIZED ANTENNA

2.1. Antenna Configuration

Figure 1 shows the configuration of the proposed compact, wideband dual-polarized multi-dipole antenna. The proposed antenna is composed of a pair of crossed SLDs, a pair of crossed RLDs, two big Y-shaped feeding lines, four small Y-shaped feeding lines, two metal pins, two 50- Ω coaxial cables, and a square metal ground plane. Both the crossed SLDs and small Y-shaped feeding lines are etched on the bottom side of an FR4 substrate ($\epsilon_r = 4.4$, $\tan \delta = 0.02$, and thickness = 0.8 mm). As seen in Figure 1(c), one small Y-shaped feeding line is extended from one arm of the crossed SLDs. The crossed RLDs and big Y-shaped feeding lines are printed on the upper side of the same FR4 substrate. To prevent overlapping from the big Y-shaped feeding lines, the feeding line in the $+45^\circ$ diagonal is divided into three parts, and one of them is shifted to the bottom side of the substrate. Then, two metal vias are utilized to connect three parts of the feeding line, as shown in Figure 1(d). Two ports, named as port 1 and port 2, are adopted to excite the proposed antenna through coaxial cables for realizing dual polarizations. The inner conductors of the coaxial cables are connected to the big Y-shaped feeding lines through the holes drilled in the substrate whereas their outer conductors are soldered on the arms of the crossed SLDs and metal ground plane. In Figure 1(b), it can be seen that the antenna radiating element is supported by four plastic posts and placed above a square metal ground plane to obtain a unidirectional radiation. Besides, two metal pins are introduced to work as baluns for balance-to-unbalance transformer. Note that two ends of each metal pin are soldered on the radiator and metal ground plane, respectively. Under the help of Ansys HFSS v.16, the design parameters are listed in Table 1.

Table 1. Optimized dimensions of the proposed antenna (unit: mm).

parameter	L_g	L_d	L_1	L_2	L_{f1}	L_{f2}	L_{f3}	L_{f4}
value	140	60	24.5	16.2	7.4	5.2	5.4	2.7
parameter	L_{k1}	L_{k2}	L_{k3}	W_s	W_t	W_1	W_2	W_{f1}
value	1	4.2	1.6	0.8	1.2	2	6.8	1
parameter	W_{f2}	W_{f3}	W_{k1}	W_{k2}	W_{k3}	W_{k4}	R	H
value	1.8	1.3	0.8	1.5	1.2	1.5	3.2	36

2.2. Design Analysis

Figure 2 displays a comparison of the impedance bandwidth with and without RLDs for the antenna when port 1 is excited. It can be seen that there are two resonant modes at 1.8 and 2.3 GHz, respectively, without loading RLDs. In this case, the impedance bandwidth is about 36.7% from 1.69 to 2.45 GHz for VSWR < 1.5 . However, it cannot cover the desired band of 1.71–2.69 GHz. To broaden the operating bandwidth, a pair of crossed RLDs and four small Y-shaped feeding lines are introduced into the design.

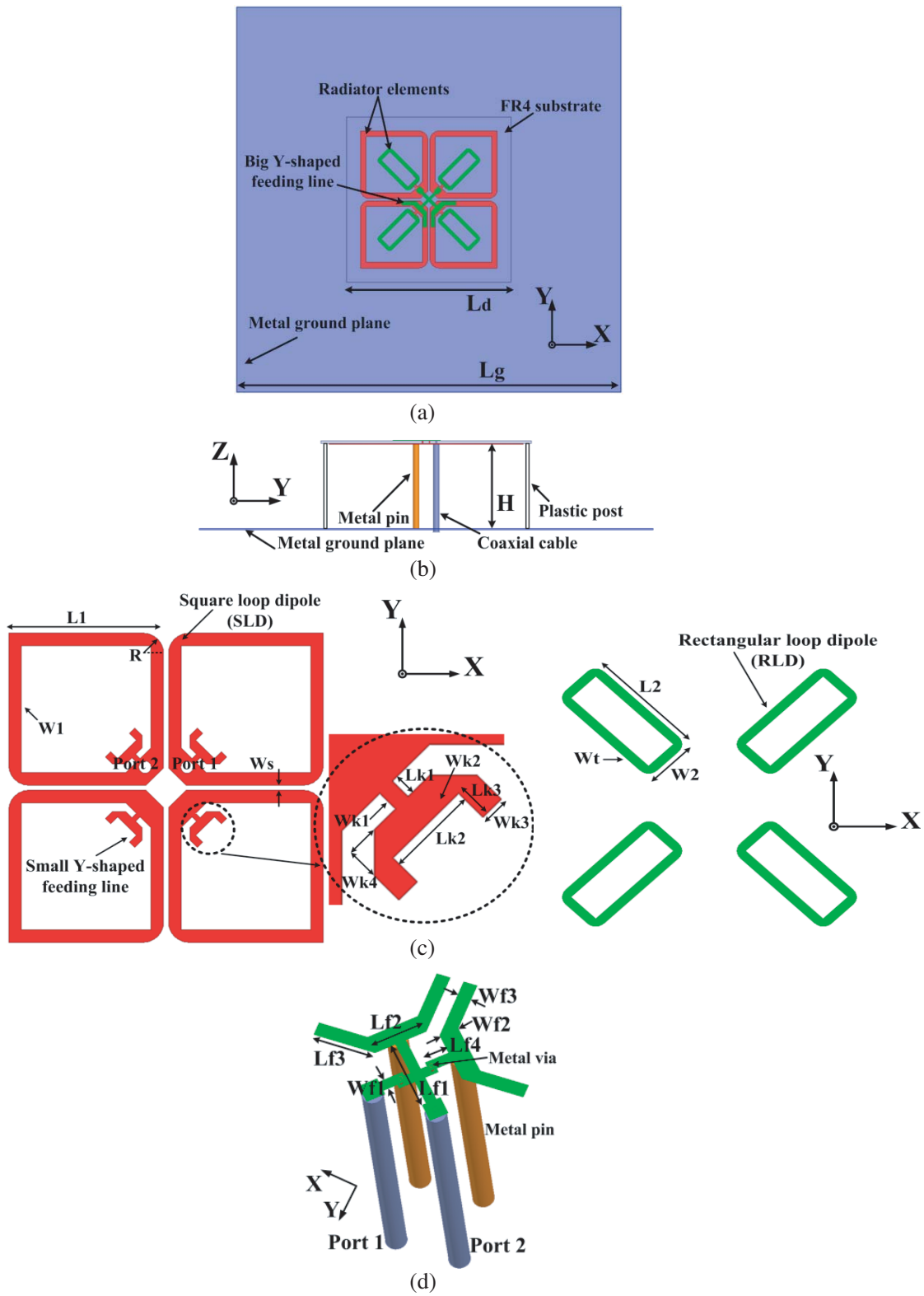


Figure 1. Configuration of the proposed dual-polarized antenna: (a) top view, (b) side view, (c) detailed view, and (d) feeding structures.

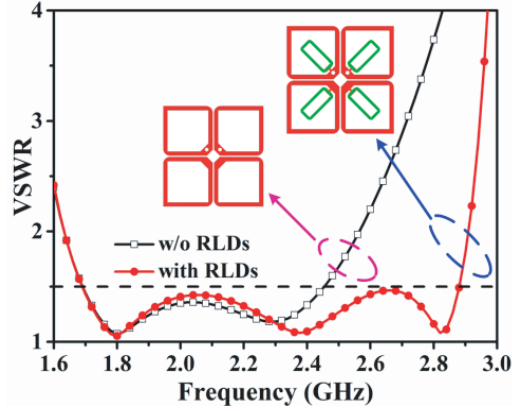


Figure 2. Simulated VSWRs of the proposed antenna with and without RLDs as the port 1 is excited.

It is observed that a new resonant mode is generated at 2.8 GHz via the capacitive coupling between the RLDs and small Y-shaped feeding lines. We also see that the original dual resonant modes are slightly affected, depicted in Figure 2. Finally, a wide impedance bandwidth from 1.69 to 2.88 GHz ($VSWR < 1.5$) is obtained for the proposed antenna after combining three resonant modes, meeting the operating bands of 2G/3G/LTE base station communication systems.

2.3. Current Distribution

Figure 3 presents the current distributions of the antenna at 1.8 and 2.8 GHz, respectively, as port 1 is excited. At low frequency of 1.8 GHz, the current is mainly concentrated on the excited SLD. In this case, the unexcited SLD and RLDs are viewed as parasitic elements, and there are some currents on

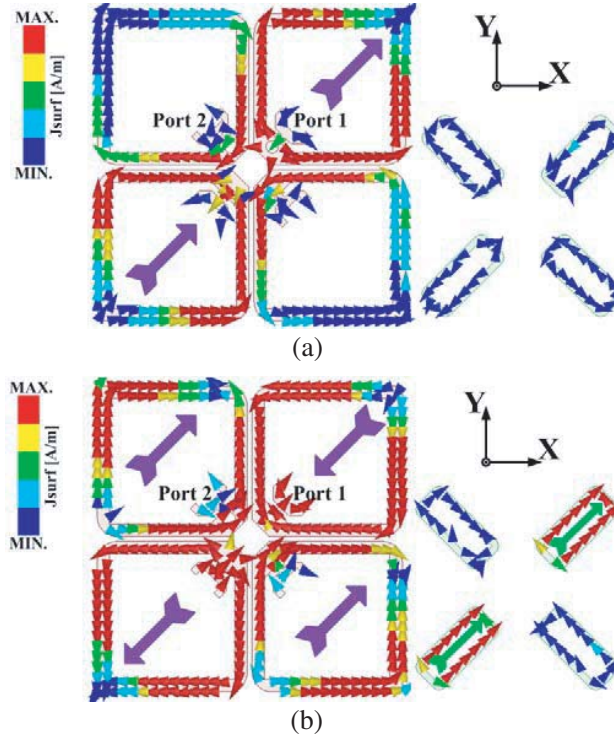


Figure 3. Current distributions of the proposed antenna at (a) 1.8 GHz and (b) 2.8 GHz as the port 1 is excited.

them. Thus, the excited SLD determines the resonant modes at 1.8 GHz. At high frequency of 2.8 GHz, there are strong currents on the SLDs and excited RLD. However, it is observed that the currents on the excited and unexcited SLDs have opposite directions, as shown in Figure 3(b). So, they have some contributions on radiating electromagnetic energy outside. In addition, the currents on the unexcited RLD are weak. Finally, a new resonant mode is generated at 2.8 GHz due to the excited RLD.

2.4. Parametric Study

To better understand the design guideline of the proposed antenna, some design parameters, affecting the operating impedance bandwidth, are studied. Note that the other design parameters remain the optimized values shown in Table 1 when one parameter is studied at a time.

The effect of parameter L_1 on the VSWR is displayed in Figure 4. It is observed that the resonant modes in the low and middle frequency bands are significantly affected by L_1 , and they gradually shift toward the lower frequency band as L_1 increases. This is because increasing L_1 will extend the physical length of the SLD, which can determine the resonant modes. However, there is a little influence on the resonant mode at high frequency. In addition, the curves in the high frequency band go up as L_1 increases, showing that the impedance matching becomes worse. Finally, $L_1 = 24.5$ mm is chosen to obtain a wide operating band with good impedance matching.

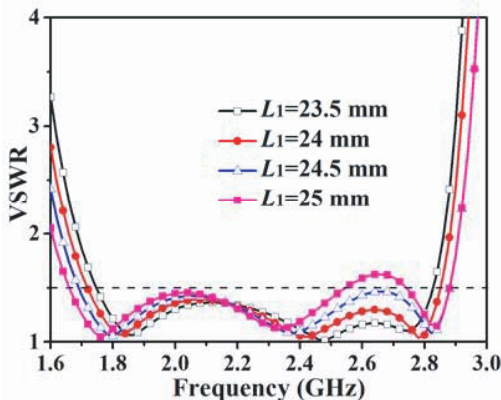


Figure 4. Simulated VSWRs versus parameter L_1 .

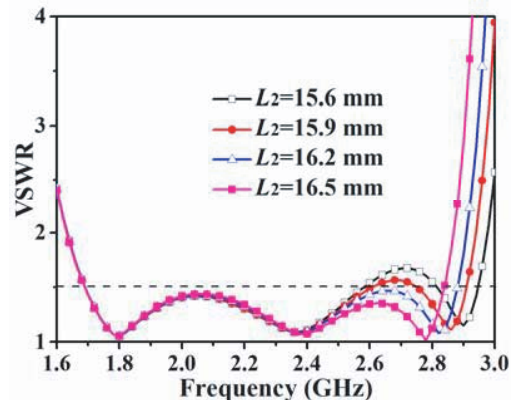


Figure 5. Simulated VSWRs versus parameter L_2 .

The effect of parameter L_2 on the VSWR is displayed in Figure 5. As L_2 increases, it can be seen that the resonant mode at high frequency moves to the lower frequency band little by little. It can be explained that parameter L_2 extends the current path of the resonant mode at high frequency. Moreover, there is a little effect on the other resonant modes within the desired operating band. Finally, $L_2 = 16.2$ mm is chosen for obtaining a wide impedance bandwidth.

The effect of parameter R on the VSWR is displayed in Figure 6. As R increases, it can be observed that the resonant mode at low frequency shifts toward the lower frequency band while the resonant mode at middle frequency moves to the higher frequency band. This is because the coupling between the excited and unexcited SLDs is reduced, resulting in the resonant modes away from each other. Thus, a compact radiator size is achieved, which can play an important role in the base station antenna array for reducing mutual coupling among the antenna elements. In addition, the resonant mode in the higher frequency band remains stable. We also see that the curves in the lower frequency band rise but go down in the higher frequency band as R increases, meaning that the impedance matching becomes gradually worse in the lower frequency band but better in the higher frequency band. Finally, $R = 3.2$ mm is chosen for implementing a broad impedance bandwidth with superior impedance matching.

The effect of parameter H on the VSWR is displayed in Figure 7. It can be seen that the impedance matching of the antenna is largely affected by parameter H . The curves gradually go down across the whole band of operation when H increases, which illustrates that the impedance matching of the proposed antenna becomes better. Finally, $H = 36$ mm is selected for ameliorating impedance matching.

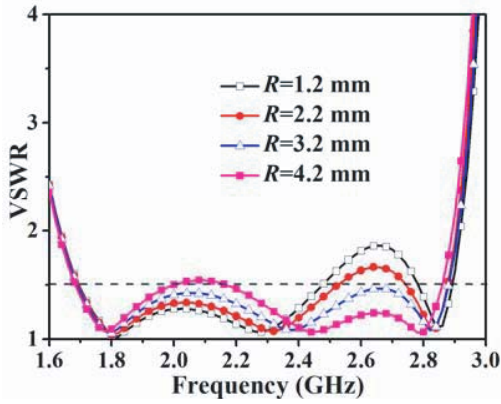


Figure 6. Simulated VSWRs versus parameter R .

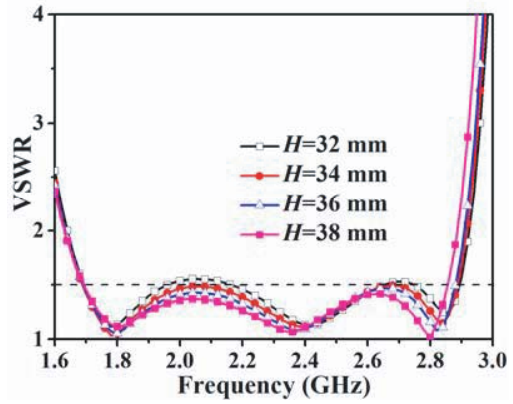


Figure 7. Simulated VSWRs versus parameter H .

3. EXPERIMENTAL RESULTS

According to the final optimized dimensions, a prototype of the proposed antenna is fabricated and measured to validate the operational performances, as shown in Figure 8. Here, a WILTRON 37269A vector network analyzer is used to measure the VSWR and port isolation. In addition, a SATIMO multi-probe spherical near field system is adopted to measure the radiation pattern and antenna gain. Figure 9 displays the simulated and measured VSWRs and port isolations of the proposed antenna. It can be seen that the simulated and measured impedance bandwidths are of 52.1% (1.69–2.88 GHz) and 53.9% (1.68–2.92 GHz), respectively, at two ports for VSWR < 1.5. Moreover, the measured port isolation of the proposed antenna is better than 30 dB across the whole operating band. We also see that

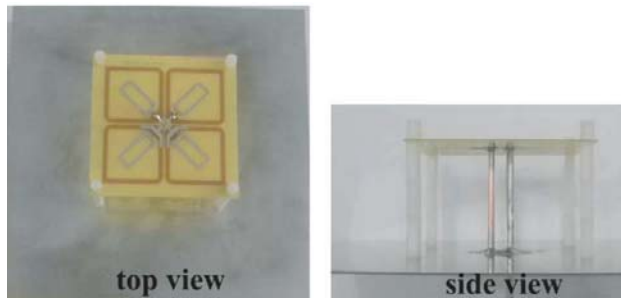


Figure 8. Photo of the proposed antenna prototype.

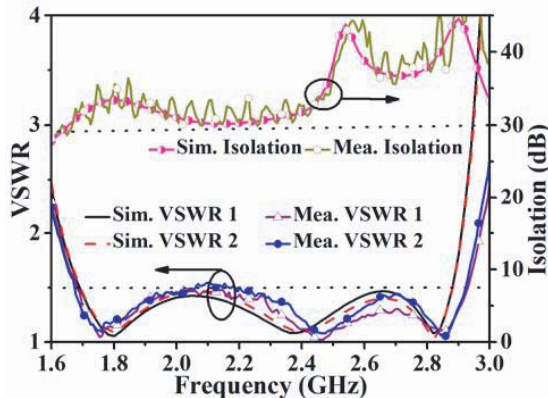


Figure 9. Simulated and measured VSWRs and isolations of the proposed antenna.

there is a little discrepancy between the simulated and measured VSWRs and port-to-port isolations, which can be attributed to fabrication tolerance and accuracy of the vector network analyzer.

The simulated and measured radiation patterns of the proposed antenna at different frequencies are depicted in Figure 10. Based on the position of the antenna in base station application, the xoz -plane is defined as the horizontal plane (H -plane) and the $yo z$ -plane defined as the vertical plane (V -plane), respectively. For simplicity, only the radiation patterns of $+45^\circ$ polarization are displayed because

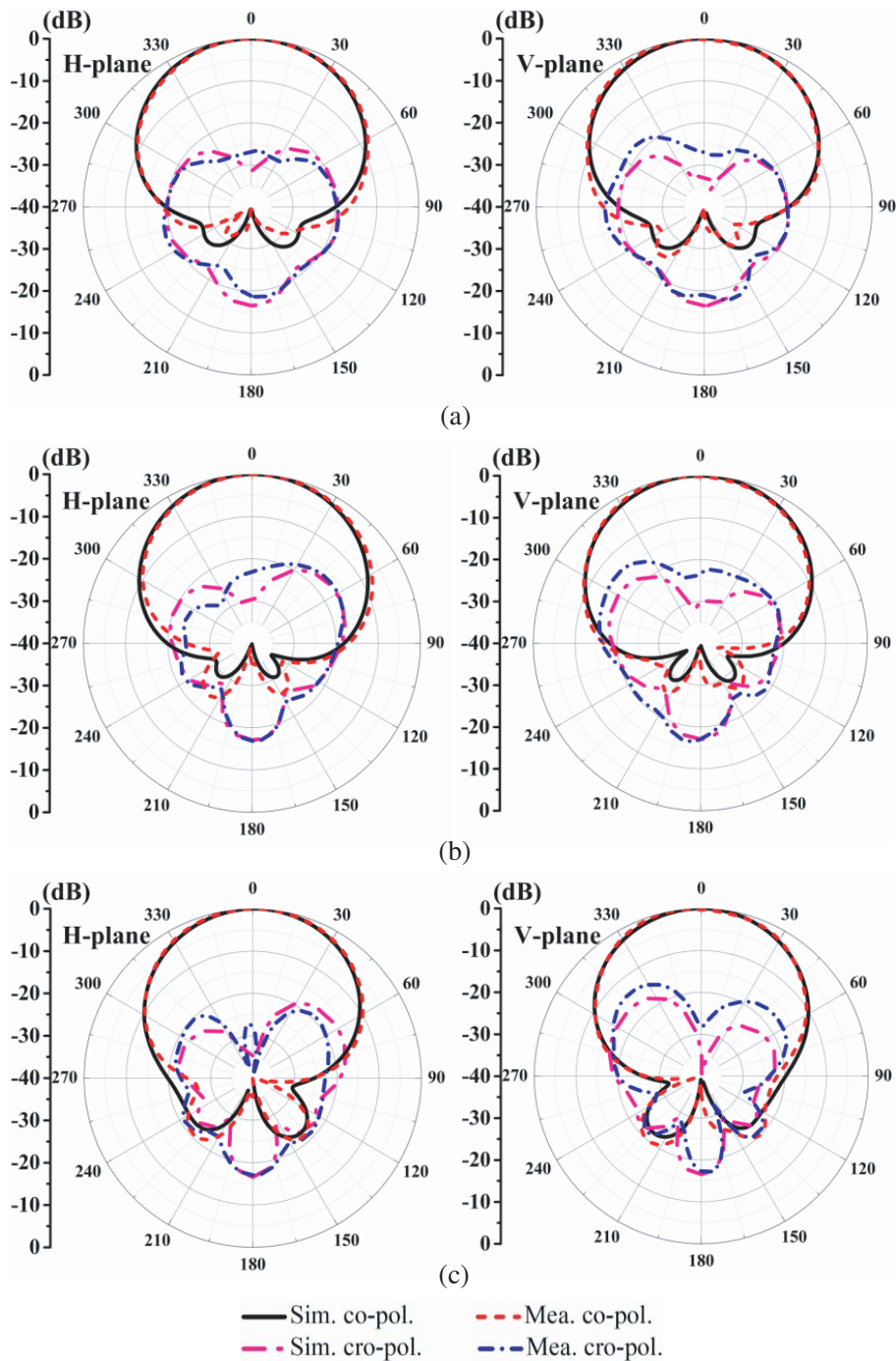


Figure 10. Radiation patterns of the proposed antenna as the port 1 is excited at (a) 1.7 GHz, (b) 2.2 GHz, and (c) 2.7 GHz.

of the symmetric structure of the proposed antenna. It can be seen that there is a good agreement between the simulated and measured radiation patterns. Measured results illustrate that the radiation pattern of the proposed antenna remains stable within the desired operating band. In addition, the cross-polarization level is less than -22 dB at boresight.

The simulated and measured gains and HPBW in H -plane are displayed in Figure 11. It can be seen that the measured antenna gains around 8.2 ± 0.5 dBi are obtained over the entire operating band for dual polarizations. Moreover, the HPBWs implemented are around $66^\circ \pm 4^\circ$ in H -plane within the operating band for the proposed antenna.

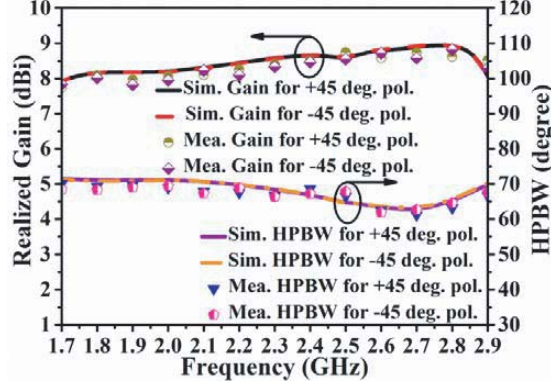


Figure 11. Simulated and measured gains and HPBWs of the proposed antenna.

Table 2. Comparison of the proposed and reported antennas.

Ref.	Bandwidth (GHz)	Radiator size (λ_0^2)	Isolation (dB)	Gain (dBi)	HPBW (degree)
[2]	1.7–2.7 ($ S_{11} < -15$ dB)	0.42×0.42	> 30	~ 8.5	~ 65
[3]	1.7–2.7 (VSWR < 1.5)	0.392×0.392	> 25	8.2 ± 0.6	68 ± 2
[6]	1.68–2.74 ($ S_{11} < -15$ dB)	0.441×0.441	> 22	~ 8.2	62 ± 4
[7]	1.7–2.9 (VSWR $< 1.5R$)	0.51×0.51	> 35	7.8 ± 0.8	NG
[11]	0.92–1.92 ($ S_{11} < -10$ dB)	0.597×0.597	> 36	8.1 ± 1.5	NG
[12]	1.72–3.4 (VSWR < 2)	0.51×0.51	> 36	~ 9.5	61.5 ± 3.5
[13]	1.7–2.7 (VSWR < 1.5)	0.805×0.805	> 39	8 ± 0.7	65 ± 4
[14]	1.56–2.73 ($ S_{11} < -10$ dB)	0.429×0.429	> 26	7.85 ± 0.75	NG
Pro.	1.68–2.92 (VSWR < 1.5)	0.382×0.382	> 30	8.2 ± 0.5	66 ± 4

NG: not given.

A comparison between the proposed and reported antennas is shown in Table 2. It can be seen that the measured impedance bandwidth of the proposed antenna is larger than those in [2, 3, 6, 13], comparable to that in [7], and smaller than those in [11, 12, 14]. However, antennas in [11, 12, 14] cannot meet the requirement of VSWR < 1.5 , which is an important index for base station applications. Besides, the radiator size of the proposed antenna is about $0.382\lambda_0 \times 0.382\lambda_0$, which is smaller than those in [2, 3, 6, 7, 11–14]. We also see that the proposed antenna has a higher port isolation than those in [3, 6, 14] and a more stable gain than those in [3, 7, 11, 13, 14]. In addition, the radiation pattern remains stable across the entire operating band. Generally, our work has a wide operating band, compact radiator size, high port isolation, stable antenna gain, and stable radiation pattern. Based on the superior performances mentioned above, the proposed antenna can be used not only in the base station applications but also in the compressive-sensing-based diagnostics applications [15].

4. CONCLUSION

In this paper, a wideband dual-polarized multi-dipole antenna with a compact radiator size is developed, fabricated, and tested. Owing to the circular chamfers in the crossed SLDs, the radiator size is reduced. By loading a pair of crossed RLDs and additional four small Y-shaped feeding lines, the operating impedance bandwidth of the proposed antenna is significantly enhanced. Measured results show that the proposed antenna has a compact radiator size of $0.382\lambda_0 \times 0.382\lambda_0$, which will help reduce mutual coupling among the antenna elements for the base station antenna array. Moreover, it has a common wide impedance bandwidth of 53.9% (1.68–2.92 GHz) for $VSWR < 1.5$ at two ports. The measured port isolation of the proposed antenna is better than 30 dB. Also, the cross-polarization level is less than -22 dB at boresight over the entire operating band. Based on the experimental results mentioned above, it can be concluded that the proposed antenna element is suitable for 2G/3G/LTE base station applications.

REFERENCES

1. Wong, K. L., *Compact and Broadband Microstrip Antennas*, Wiley, Hoboken, NJ, USA, 2002.
2. Cui, Y. H., R. L. Li, and H. Z. Fu, "A broadband dual-polarized planar antenna for 2G/3G/LTE base stations," *IEEE Transactions on Antennas and Propagation*, Vol. 62, No. 9, 4836–4840, 2014.
3. Chu, Q. X., D. L. Wen, and Y. Luo, "A broadband $\pm 45^\circ$ dual-polarized antenna with Y-shaped feeding lines," *IEEE Transactions on Antennas and Propagation*, Vol. 63, No. 2, 483–490, 2015.
4. Wu, J. J., W. Yu, and J. Chen, "A broadband dual-polarized arm-overlapped dipole antenna for base station applications," *Progress In Electromagnetics Research C*, Vol. 89, 51–59, 2019.
5. He, H., Y. Liu, and S. X. Gong, "A broadband dual-polarized base station antenna with anti-interference capability," *IEEE Antennas Wireless Propagation Letters*, Vol. 16, 613–616, 2017.
6. He, H., Y. Liu, and S. X. Gong, "A broadband dual-polarized base station antenna with sturdy construction," *IEEE Antennas Wireless Propagation Letters*, Vol. 16, 665–668, 2017.
7. Gou, Y. S., S. W. Yang, J. X. Li, and Z. P. Nie, "A compact dual-polarized printed dipole antenna with high isolation for wideband base station applications," *IEEE Transactions on Antennas and Propagation*, Vol. 62, No. 8, 4392–4395, 2014.
8. Lai, H. W. and K. M. Luk, "Dual polarized patch antenna fed by meandering probes," *IEEE Transactions on Antennas and Propagation*, Vol. 55, No. 9, 2625–2627, 2007.
9. Wang, Y. and Z. W. Du, "Dual-polarized slot-coupled microstrip antenna array with stable active element pattern," *IEEE Transactions on Antennas and Propagation*, Vol. 63, No. 9, 4239–4244, 2015.
10. Feng, B. T., W. X. An, S. X. Yin, L. Deng, and S. F. Li, "Dual-wideband complementary antenna with a dual-layer cross-ME-dipole structure for 2G/3G/LTE/WLAN applications," *IEEE Antennas Wireless Propagation Letters*, Vol. 14, 626–629, 2015.
11. Xue, Q., S. W. Liao, and J. H. Xu, "A differentially-driven dual-polarized magneto-electric dipole antenna," *IEEE Transactions on Antennas and Propagation*, Vol. 61, No. 1, 425–430, 2013.
12. Wu, B. Q. and K. M. Luk, "A broadband dual-polarized magneto-electric dipole antenna with simple feeds," *IEEE Antennas Wireless Propagation Letters*, Vol. 8, 60–63, 2009.
13. Luo, Y. and Q. X. Chu, "Oriental crown-shaped differentially fed dual-polarized multidipole antenna," *IEEE Transactions on Antennas and Propagation*, Vol. 63, No. 11, 4678–4685, 2015.
14. Zhou, C. F., H. Wong, and L. K. Yeung, "A wideband dual-polarized inductor-end slot antenna with stable beamwidth," *IEEE Antennas Wireless Propagation Letters*, Vol. 17, No. 4, 608–612, 2018.
15. Morabito, A. F., R. Palmeri, and T. Isernia, "A compressive-sensing-inspired procedure for array antenna diagnostics by a small number of phaseless measurements," *IEEE Transactions on Antennas and Propagation*, Vol. 64, No. 7, 3260–3265, 2016.